**Project Title:** Advanced Boron and Metal Loaded High Porosity Carbons

**Project Period:** February 1, 2005 to January 31, 2010
**Recipient:** Pennsylvania State University
**Award Number:** DE-FC36-05GO15077

**Working Partners:**

Peter C. Eklund (deceased)
T. C. Mike Chung
Henry C. Foley
Vincent H. Crespi

**Cost-Sharing Partners:** NA

**Contact:** Vincent H. Crespi
104 Davey Lab MB 193
University Park, PA 16802
vhc2@psu.edu
814 863-0163
814 865-3604 (fax)

**DOE Managers:**

DOE HQ Technology Manager: Carole Read
DOE Field Project Officer: Jesse Adams

## Executive Summary:

The Penn State effort explored the development of new high-surface-area materials for hydrogen storage, materials that could offer enhancement in the hydrogen binding energy through a direct chemical modification of the framework in high specific-surface-area platforms. The team chemically substituted boron into the hexagonal $sp^2$ carbon framework, dispersed metal atoms bound to the boro-carbon structure, and generated the theory of novel nanoscale geometries that can enhance storage through chemical frustration, sheet curvature, electron deficiency, large local fields and mixed hybridization states. New boro-carbon materials were synthesized by high temperature plasma, pyrolysis of boron-carbon precursor molecules, and post-synthesis modification of carbons. Hydrogen uptake has been assessed, and several promising leads have been identified, with the requirement to simultaneously optimize total surface area while maintaining the enhanced hydrogen binding energies already demonstrated.

## Comparison of accomplishments with goals:

The ultimate, ideal goal was to obtain materials that met the DOE targets for gravimetric and volumetric storage at reasonable cost. As enabling accomplishments on the path towards these goals, the project focussed on developing new methods of synthesizing and characterizing high surface area materials using a modified framework that bound

hydrogen with energies in excess of those previously known for physical adsorption. In addition, one project goal was to develop novel via theory lines of inquiry into obtaining enhance adsorption while maintaining the favorable kinetics and heat management of physical adsorption, such as spillover, electron deficiency, crystalline open zwitterions, aggregation-resistance and reversible framework aminobenzenes, etc. The project was successful in meeting these enabling accomplishments, including significant enhancement in hydrogen binding energies, although the ambitious DOE storage targets were not met (by this or any other project, to our knowledge). Please refer to the Center database for specific information on storage capacities, etc.

**Summary of project activities and outcomes:**

The following table provides a summary of project goals through the life of the project. Goals 1 – 10 were fully met. Later goals were met at the 75% level overall. Detailed discussion of each of these activities and outcomes is provided later in this report and also in the regular quarterly reports.

| | |
|---|---|
| 1 | Develop synthesis protocols and apparati for incorporation of boron into carbons |
| 2 | Computational design of first candidate nanoscale structures for enhanced binding |
| 3 | Demonstrate that boron is substitutionally doped in sp2 carbons |
| 4 | First measurements of hydrogen binding in novel boro-carbons |
| 5 | Production of boron-substituted carbons with at least 5% boron |
| 6 | Differential volumetric apparatus designed, fabricated, tested |
| 7 | Development of high-throughput electrochemical screening for hydrogen storage samples |
| 8 | First production of metal-boro-carbons |
| 9 | Production of boron-substituted carbons with at least 10% boron |
| 10 | Computational design of multiple candidate structures for enhanced binding, using distinct mechanisms of enhancement |
| 11 | Determination of best elemental metal for metal-boro-carbons |
| 12 | Determination of maximal molecular hydrogen binding in (metal)-boro-carbons |
| 13 | Computational design of high SSA, high binding, thermodynamically stable sorbents |
| 14 | Determination of maximal specific surface area of enhanced (metal)-boro-carbons |
| 15 | Fundamental studies of spillover mechanism on graphene systems |
| 16 | Optimization of new systems from 10 |

**Computer modeling:**

Density functional theory in the local density approximation and generalized gradient approximation was used for a wide range of efforts in materials design of new candidate mechanisms for enhance hydrogen physical adsorption. The key assumption is that the enhancement will be arise from a strengthening of the van der Waals component of the interaction, since this component is absent at this level of theory, but instead from charge transfer, hybridization, polarization, and other mechanisms that are amenable to treatment within this computational scheme. Density functional theory has been well-tested over decades in the peer-reviewed literature – literally thousands of validation studies with intensive comparison to experiment – for these physical interactions and it provides a reasonably accurate and general framework, the best currently available for

systems of this size and complexity. The code VASP was used for the bulk of these calculations. This code is publicly available from the Vienna electronic structure group.

**Main Discussion:**

Turning to the detailed technical description of accomplishments, the Penn State group has made significant advances in a precursor approach to preparing $BC_x$ materials with controlled B content and morphology (i.e. surface area). The idea is based on the thinking that B has similar atomic size as C and B forms a strong tri-valence bonding structure with C. Therefore, it is possible that B can be effectively substituted in the C (grapheme) structure without significantly distorting its planar structure. In fact, there are some existing organoborane compounds that have similar B-substituted fused-ring structures. The key concept here is to design suitable B-precursors that can be thermally transformed into a fused ring structure without losing the B and C elements. At the same time, the precursors must create a micro-porous structure with high surface area in the resulting $BC_x$ material. It is highly desirable to have strong acidic B moieties (i.e. electron deficiency) in the resulting $BC_x$, which shall engage in π-electron delocalization in the fused-ring structures and serve as p-type internal dopants to activate the surfaces and increase the $H_2$ binding energy.

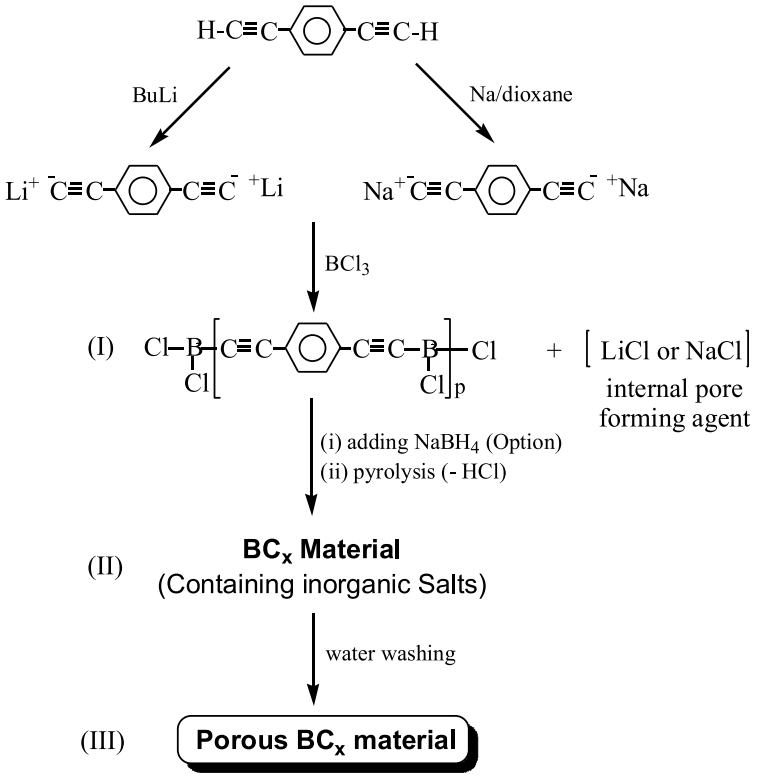


**Equation 1:** Synthesis route for preparing porous $BC_x$ materials.

Several organic and polymeric B-precursors were designed and synthesized and then subjected to pyrolysis procedure to form $BC_x$ materials. One successful example is poly (diethynylphenylborane chloride) (I), as illustrated in Equation 1. In this B-precursor (I), the combination of alkynyl and B-Cl moieties is very favorable for inter-polymer reactions at low temperature (<150°C), which involve chloroboration and cyclization.

The precursor (I) changes color from white to brown, also increasing molecular mass without losing weight. Both reactions offer an important stabilization step to assure a high pyrolysis yield at high temperatures. Beyond 150°C, the precursor quickly deepens in color with the continuous evolution of HCl gas, which may be related to an electrophilic substitution on aromatic rings involving B-Cl moieties to incorporate B in the fused ring structures. After initial weight loss up to 400°C — mostly due to the HCl by-product — the weight loss becomes relatively small. At 600°C, the total weight loss is about 20%, which is close to the expected value when removing all H and Cl atoms in the B-precursor (I). In fact, the PGAA measurement of the resulting porous $BC_x$ material (III) — after water-washing to remove LiCl salts — shows almost only B and C elements in a $BC_{11}$ composition. This material possesses 7.7 wt% of B, which is only slightly below 8.4 wt% in the starting B-precursor (I) (only considering B and C contents).

During the polycondensation reaction (Equation 1), the *in situ* formed inorganic salts (LiCl or NaCl) are insoluble in solvent (hexane or dioxane) and are co-precipitated out with the resulting high molecular weight B-precursor (homogeneous solid). In subsequent pyrolysis, the B-precursor (I) involves a facile thermal transformation to form a $BC_x$ fused ring structure; in the meantime, LiCl or NaCl salts are inert and serve as the pore-forming templates (removed after pyrolysis by water-washing) to produce porous $BC_x$ morphology. The resulting porous structure in the $BC_x$ material essentially mirrors the structure of the impregnated inorganic aggregates in the matrix.

**Table 1**: A summary of porous $BC_x$ materials prepared by B-precursor containing inorganic salts under various pyrolysis conditions

| Run No. | Pore-forming Additives | Pyrolysis Temp. (°C) | B Content (wt%) | | Surface Area ($m^2/g$) | Composition ($BC_x$) |
|---|---|---|---|---|---|---|
| | | | $^{11}B$ NMR | PGAA | | |
| A-1 | LiCl | 600 | 7.7 | 7.7 | 780 | $BC_{11}$ |
| A-2 | LiCl | 800 | 6.4 | 6.0 | 528 | $BC_{13}$ |
| A-3 | LiCl | 1100 | 4.2 | - | - | $BC_{21}$ |
| A-4 | LiCl | 1400 | 3.5 | 3.7 | - | $BC_{25}$ |
| A-5 | LiCl | 1500 | 2.6 | - | 36 | $BC_{34}$ |
| A-6 | LiCl | 1800 | 2.2 | 2.0 | - | $BC_{40}$ |
| B-1 | NaCl | 600 | 6.5 | - | 634 | $BC_{13}$ |
| B-2 | NaCl | 900 | 5.2 | - | - | $BC_{17}$ |
| C-1 | LiCl + $NaBH_4$ | 600 | 12.2 | 12.8 | 609 | $BC_6$ |
| C-2 | LiCl + $NaBH_4$ | 800 | 10.4 | 9.2 | - | $BC_8$ |

Table 1 summarizes several resulting porous $BC_x$ materials prepared by boron-containing polymeric precursor (B-precursor) under various pyrolysis conditions. The B-precursor contains various inorganic salts (pore-forming additives) that were removed by water-washing after pyrolysis. Comparing A set, the B content slowly decreases with the further increase of the pyrolysis temperature. The composition

changed from $BC_{11}$ at 600 °C to $BC_{13}$ and $BC_{21}$ at 800 and 1100 °C, respectively. The evolution of the $BC_x$ composition coincides with the development of it planar fused ring structure and crystallinity. The composition becomes quite constant after 1500 °C, with slightly above 2 wt% B content that is close to the reported maximum value of substitutional B content in the crystalline graphite structure. The addition of external additives, such as $NaBH_4$, can significantly increase B content at a low temperature (600-1000 °C range). However, after pyrolysis at 1500 °C the resulting $BC_x$ materials also exhibit <3 mol% B content.

The molecular structure of BCx materials during the pyrolysis was monitored by a combination of solid state $^{11}B$ MAS-NMR, X-ray diffrraction, and TEM micrograph. Figure 1 shows the $^{11}B$ MAS-NMR spectra of several resulting porous $BC_x$ materials, which were prepared by pyrolysis of B-precursor containing *in situ* formed LiCl salts at various temperatures, then subsequent water-washing to remove all LiCl additives. After pyrolysis at 600 °C, the resulting porous $BC_{11}$ (run A-1) shows one distinctive broad chemical shift centered at 10 ppm, corresponding to trivalent B moieties that involve some π-electron delocalization in the C fused rings. There is a minor peak centered at 0 ppm, which may be associated with few B moieties located at the edge area of the porous $BC_{11}$ structure. During water-washing, the remaining B-Cl groups should change to B-OH groups. As the pyrolysis temperature increases from 600 to 800 °C, the major trivalent B peak slowly moves up-field, indicating gradually increase of electron density at B and better π-electron conjugation in the $BC_{13}$ material (run A-2). On the other hand, the edge area B moieties sharply decrease in its intensity. At 1100 °C, only a trivalent B peak at 8 ppm was observed in $BC_{21}$ (run A-3). Evidently, the $BC_x$ fused ring structure increases its size as the pyrolysis temperature increases, and most of B moieties become the substitutional trivalent species inside the $BC_x$ structure. Further annealing the sample at higher temperatures (1500 ˚C), the $BC_x$ material appears to graphitize on a larger scale, with a single B chemical shift abruptly moving up-field to -5 ppm in the $BC_{28}$ material (run A-5), which indicates that B is highly involved in π-electron delocalization to form very weak acidic (or even basic) B moieties.

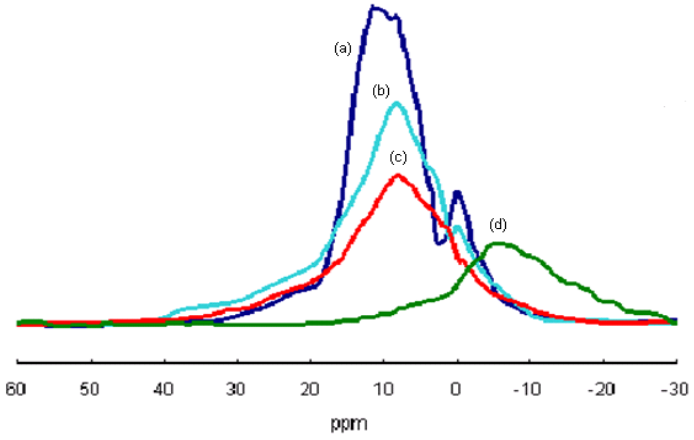


**Figure 1:** Solid state (MAS) $^{11}B$ NMR spectra of $BC_x$ materials prepared from pyrolysis of B-precursor (with LiCl salts) at (a) 600 °C (run A-1), (b) 800 °C (run A-2), (c) 1100 °C (run A-3), and (d) 1500 °C (run A-5).

Table 2 summarizes the X-ray crystallite parameters of interlayer spacing (d), crystallite size (Lc), and crystallite width (La). Generally speaking, the d-spacing decreases with heat treatment temperature, while both Lc and La increase with temperature. The $BC_{11}$ sample (run A-1) is almost completely amorphous, and the $BC_x$ material gradually shows small order domains as the pyrolysis temperature increases to 1400 °C (run A-4), with two broad (100) and (101) peaks. A small amount of boron carbide ($B_4C$) was also observed at 1500 °C (run A-5). As discussed, the B content in $BC_x$ material at 1500 °C (Table 1) dramatically reduced to 2.6 wt%, which is close to the maximum B solubility level in the graphitic structure. Evidently, at this temperature, some small crystallites were formed with a short-range order structure, which ejects excess B in the form of $B_4C$ from the matrix. However, both crystallite size and crystallite width remain relatively small even after pyrolysis at 1800 °C, which may be associated with the co-existence of inorganic salts (impurities) that limit the expansion of crystallite domains and prevent the long-range order. The final $BC_x$ materials basically resemble the disordered (non-graphitizable) carbons. However, the d-spacing of run A-6 is 0.339 nm—very close to 0.335 nm in ideal graphite. Despite the relatively low pyrolysis temperature at 1800 °C, the highly short-range ordering may be associated with having B in the precursor, which enhances the graphitization process.

**Table 2:** Lattice parameters of $BC_x$ materials measured by X-ray diffraction patterns.

| Run No. | Pyrolysis Temp. (°C) | Composition ($BC_x$) | d-Spacing (nm) | La (nm) | Lc (nm) |
|---|---|---|---|---|---|
| A-1 | 600 | $BC_{11}$ | - | - | - |
| A-2 | 800 | $BC_{13}$ | 0.367 | 3.70 | 1.10 |
| A-3 | 1100 | $BC_{21}$ | 0.356 | 3.73 | 1.23 |
| A-4 | 1400 | $BC_{25}$ | 0.353 | 4.87 | 1.61 |
| A-5 | 1500 | $BC_{28}$ | 0.347 | 5.04 | 1.64 |
| A-6 | 1800 | $BC_{40}$ | 0.339 | 6.04 | 2.77 |

High-resolution TEM provided direct observation of microstructures. Figure 3 (a) and (b) compare two TEM micrographs of $BC_{11}$ (run A-1) and $BC_{40}$ (run A-6) materials. In the $BC_{11}$ material, prepared at 600°C, we observed fingerprint patterns with short and curved fringes, and randomly-oriented fringes between fingerprint patterns. On the other hand, the randomly-oriented stacks of several layers, with extended, straight, and parallel organized fringes were observed in the $BC_{40}$ material prepared at 1800°C. The stack thickness (Lc; crystallite size) is about 2-3 nm, and the stack length (crystallite width) is in the range of 5-7 nm—consistent with the X-ray results (Table 2). TEM micrograph for the $BC_6$ material (run C-1), using the B-precursor (I) containing both *in situ* formed LiCl and the externally added $NaBH_4$ salts, shows a completely random configuration (no fingeprint patterns) with short and curved fringes. Evidently, the additional $NaBH_4$ salts were mixed well with B-precursor (I), and providing an additional B source. Although they don't interfere in the carbonization process of converting B-precursor (I) into the $BC_x$ material, their presence in the matrix does

effectively prevent any development of a local ordering structure by maintaining a high edge area.

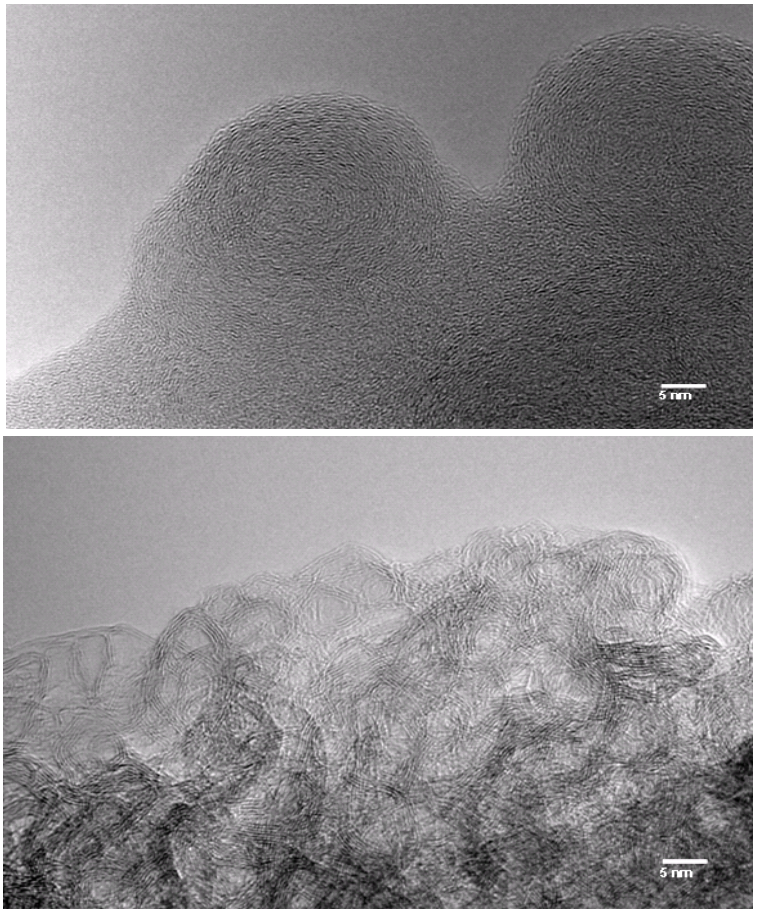


**Figure 3:** TEM micrographs of (a) $BC_{11}$ (run A-1) and (b) $BC_{40}$ (run A-6).

As illustrated in Figure 4, the chemical structure of $BC_x$ changes from a disordered (less π-conjugated) state—with a boron-puckered configuration at 600-800 $^oC$—to an ordered (highly π-conjugated) state—with a planar and mutiple-layered configuration at 1500 $^oC$. The resulting planar graphitic layers can only accommodate a reduced amount (<3%) of B content that is consistent with the previous observation.

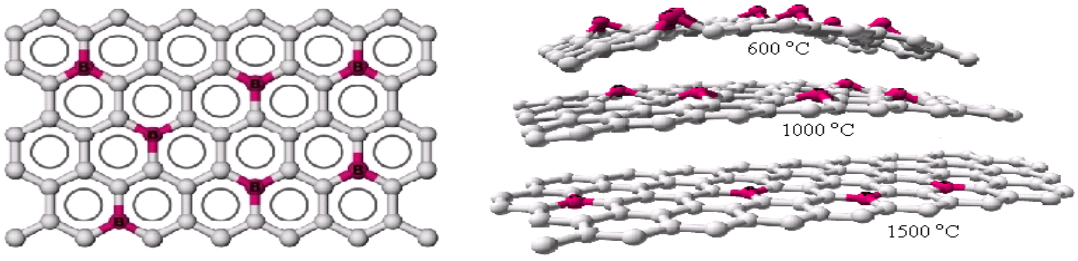


**Figure 4:** Schematic presentation of $BC_x$ materials (left) top view and (right) side view.

We have developed substantial understanding of how the pyrolysis temperature and inorganic salts affect $BC_x$ morphology. Since the inorganic additives serve as the pore-forming templates, removed after pyrolysis, the pore structure also reveals the distribution of inorganic salts in the $BC_x$ matrix during pyrolysis. Figure 5 shows SEM microscopies of three $BC_x$ materials, including $BC_{11}$ (run A-1), $BC_{40}$ (run A-6), and one control sample that was prepared by pyrolysis (600 $^oC$) of a low molecular weight pure B-precursor (I), containing no inorganic salt. Despite very different pyrolysis temperatures (600 $^oC$ vs 1800 $^oC$), both $BC_{11}$ and $BC_{40}$ materials show similar macro-phase morphology with many continuous micron-width channels (Figure 5, a and b). However, a completely dense $BC_x$ material (Figure 5, c), with almost no surface area, was observed from the same B-precursor that did not contain the LiCl salts or other additives, such as NaCl and $NaBH_4$. These macro-porous structures are clearly the result of LiCl aggregates in the matrix, which may be formed (phase separated from $BC_x$) during pyrolysis.

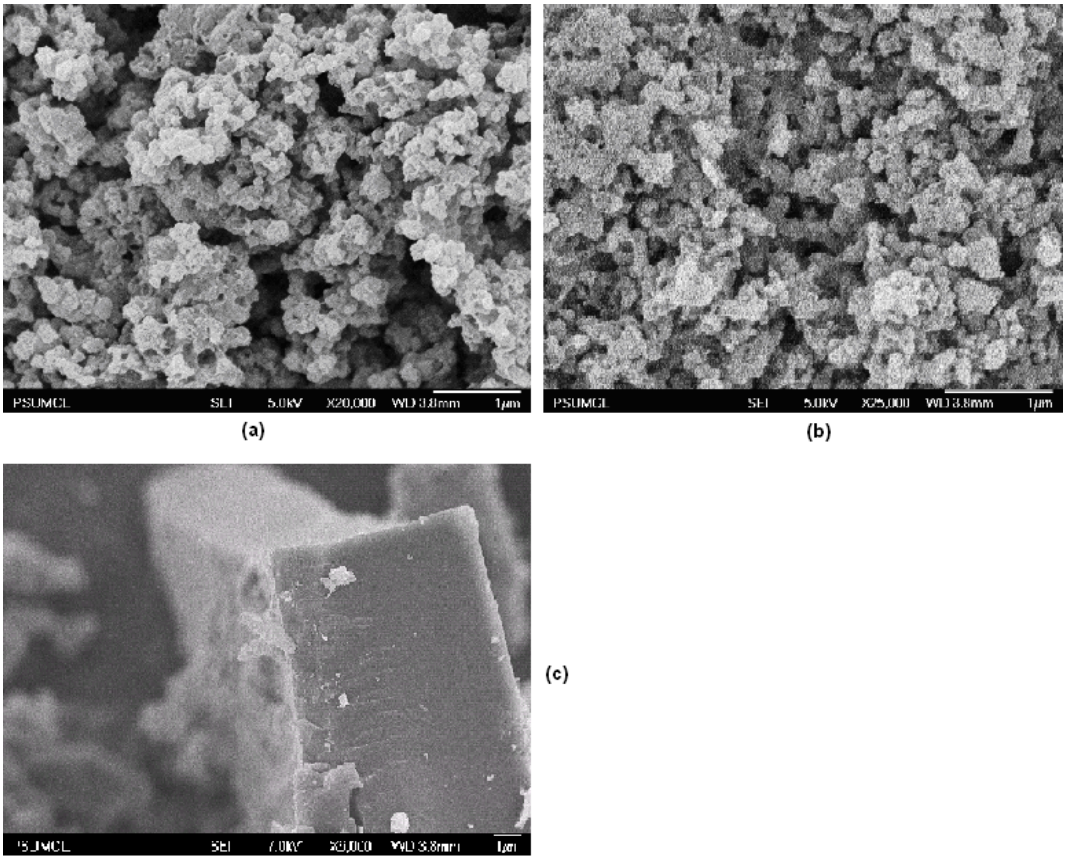


**Figure 5:** SEM micrograph of $BC_x$ materials obtained after pyrolysis of B-precursor (with LiCl) at (a) 600 $^oC$ (run A-1) and (b) 1800 $^oC$ (run A-6), and (c) B-precursor (without LiCl) at 600 $^oC$.

It is interesting to know how much LiCl salts are still dispersed in the $BC_x$ matrix, which may result in much smaller pore structures. Figure 6 shows a high-resolution FE-SEM micrograph of the same $BC_{11}$ sample (Figure 5,a). Both micropores and mesopores

clearly exist in the $BC_{11}$ matrix. However, the resolution does not allow for the determination of pore size and distribution. The specific pore sizes and pore size distributions in the $BC_x$ materials were examined by a BET surface area analyzer using $N_2$ and $CO_2$ gases.

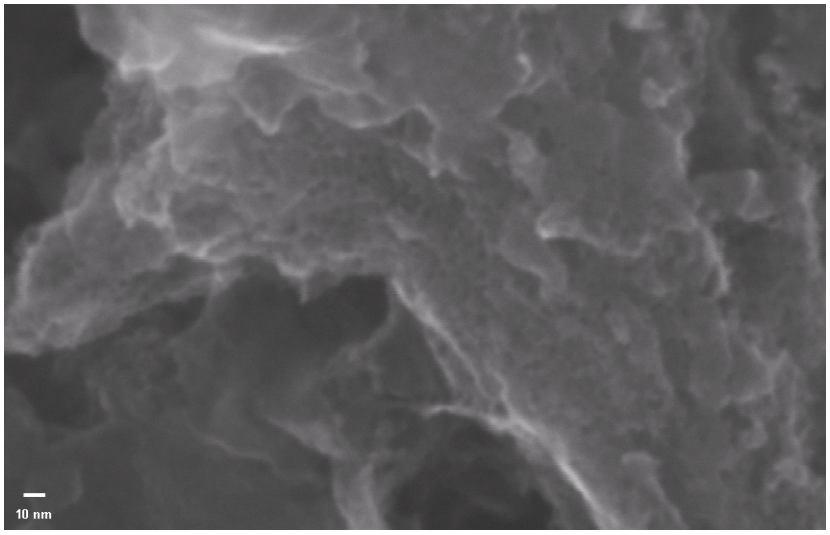


**Figure 6:** FT-SEM micrograph of $BC_{11}$ materials (run A-1).

Figure 7 compares four pore size distribution curves of $BC_{11}$ (run A-1), $BC_{13}$ (run A-2), $BC_{13}$ (run B-1), and $BC_{17}$ (run B-2), prepared by pyrolysis of the B-precursor (I) containing LiCl or NaCl salts under various pyrolysis temperatures. Table 3 summarizes their surface areas and micropore volumes that were calculated from adsorption isotherms of $N_2$ (77K) and $CO_2$ (273K) using BJH and D-R methods, respectively. It is interesting to note that the surface areas measured by $CO_2$ sorption consistently show higher values than those measured by $N_2$, especially in B-1 and B-2 samples. Since the $CO_2$ measurement is capable of covering the extremely small pores (between 3.2 and 3.6 A), both B-1 and B-2 samples prepared by NaCl impregnation may contain smaller pores (discussed later). Both A-1 and A-2 materials, obtained from B-precursor (I) with LiCl salts at 600 $^oC$ and 800 $^oC$, respectively, contain micropores (with pore diameter centered at 1.2 nm) and mesopores (with pore diameter centered at 3.75 nm), but with very different proportions. The significant shift of the micropore-dominated A-1 sample (83 vol% micropores in Figure 7 (a)) to the mesopore-dominated A-2 sample (87 vol% mesopores in Figure 7 (b)) implies some local LiCl agglomeration after pyrolysis, beyond its melting temperature at 605 $^oC$. As expected, the BET surface area also reduces from 780 to 528 $m^2/g$. The same general trend was also observed in B-1 and B-2 pair that was prepared at 600 $^oC$ and 900 $^oC$, respectively. It is interesting to see the mainly micropores in Figure 7 (c) for the $BC_{13}$ material, prepared in run B-1 with NaCl additives, and B-2 sample maintained more than half of micropores, even after heating at a significantly higher temperature. The NaCl salts, having a higher melting temperature (800 $^oC$), remain in a well-dispersed phase in the $BC_x$ matrix at 600 $^oC$. Clearly, the combination of additives and pyrolysis temperature offers a unique tool (templates) to control $BC_x$ morphology.

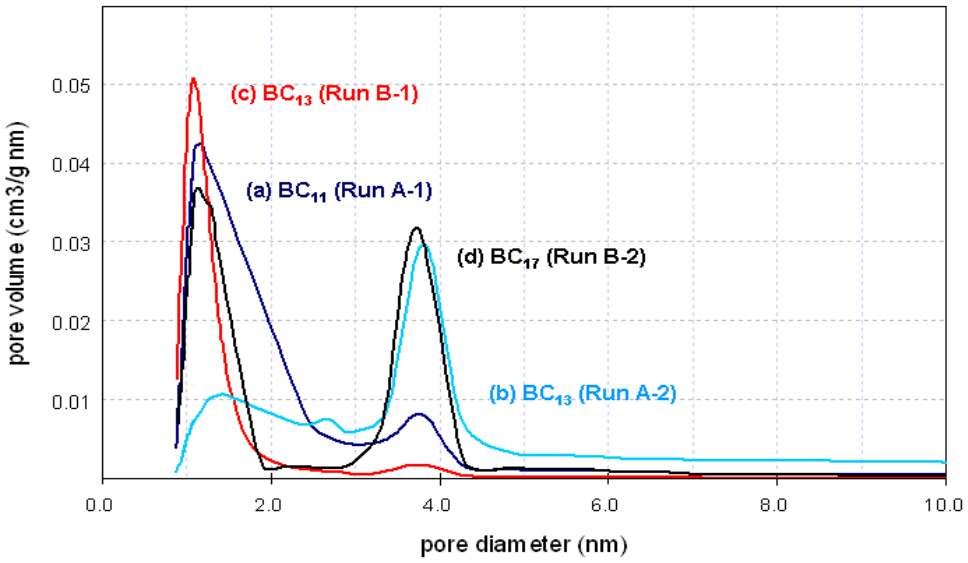


**Figure 7:** Pore size distribution of (a) $BC_{11}$ (run A-1), (b) $BC_{13}$ (run A-2), (c) $BC_{13}$ (run B-1), and (d) $BC_{17}$ (run B-2).

**Table 3:** A Summary of surface area and pore volume of four $BC_x$ materials shown in Figure 10.

| | $N_2$ sorption at 77K | | | $CO_2$ sorption at 273K | |
|---|---|---|---|---|---|
| Sample | Surface area[a] ($m^2/g$) | Micropore volume[b] ($cm^3/g$) | Desorption cumulative pore volume[b] ($cm^3/g$) | Surface area[c] ($m^2/g$) | Micropore volume[c] ($cm^3/g$) |
| A-1 | 780 | 0.38 | 0.43 | 873 | 0.33 |
| A-2 | 528 | 0.10 | 0.29 | 569 | 0.16 |
| B-1 | 634 | 0.34 | 0.34 | 828 | 0.32 |
| B-2 | 405 | 0.16 | 0.29 | 762 | 0.25 |

a. Calculated by BET equation
b. Estimated by BJH method.
c. Estimated by D-R method.

Figure 8 shows an X-ray diffraction (XRD) pattern of the impregnated LiCl during the pyrolysis of B-precursor (I), which provides the direct evidence of LiCl aggomeration at a high pyrolysis temperature. At the temperature <400 °C, the dispersed LiCl molecules show no diffraction peak. As the pyrolysis temperature increases to >450 °C, several sharp diffraction peaks suddenly appeared: they are associated with the LiCl crystals in hydrated (exposed in air) and anhydrous forms. Evidently, the dispersed LiCl molecules start to melt flow below the melting point (605 °C) of LiCl crystal, and aggregate progressively into bigger particles. It is important to note that the *in situ* formed LiCl molecules in B-precursor (I) were conveniently used as the internal pore-forming additives to prepare various porous structures in the $BC_x$ material, which can be

completely removed by water-washing. The resulting pore structure in $BC_x$ is the mirror image of the impregnated LiCl aggregates in the matrix.

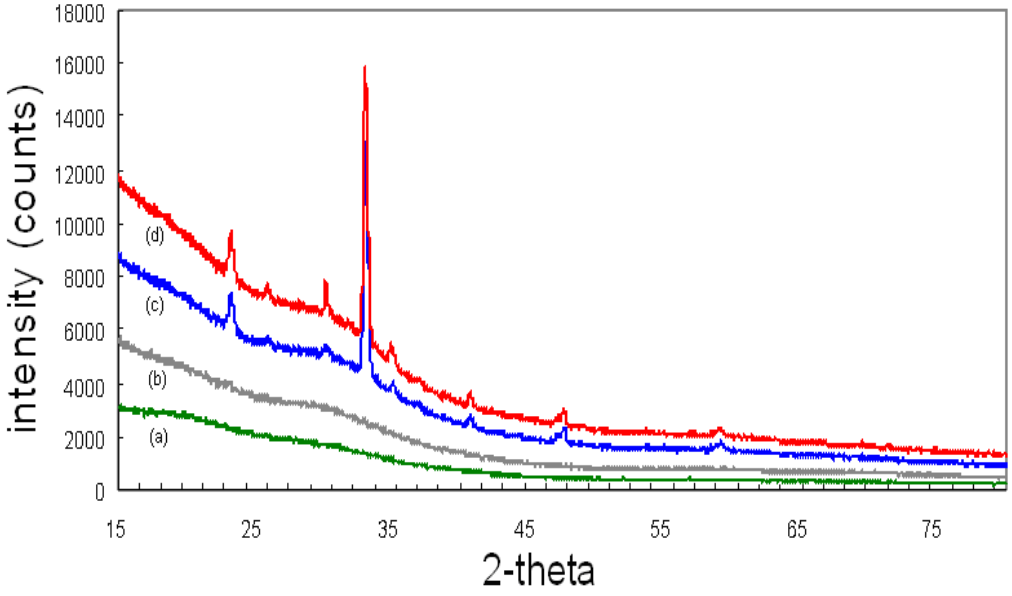


**Figure 8:** X-ray diffraction patterns of LiCl salts in B-precursor after pyrolysis at various temperatures (a) 150 °C, (b) 400 °C, (c) 450 °C, and (d) 600 °C.

The resulting porous $BC_x$ materials were examined as absorbents for hydrogen storage. Both gravimetric and volumetric hydrogen adsorption measurements were carried out under various temperatures and pressure conditions. Figure 9 shows hydrogen adsorption of $BC_{11}$ (run A-1) and $BC_6$ (run C-1) at 77K and 293 K, respectively. Hydrogen uptake almost follows a linear relationship with hydrogen pressure, which is quite different from C materials that reach a saturation level in relatively low pressure. About 0.37 wt% hydrogen adsorption was observed in the $BC_{11}$ material, having a specific surface area of 780 $m^2/g$, at ambient temperature under 80 bars $H_2$ pressure, which is about double that of carbonaceous materials with similar surface areas. Temperature has a marked effect on the increase of the hydrogen adsorption capability. At 77 K, hydrogen adsorption reaches the 3 wt % mark—more than 7 times that at ambient temperature. This value is more than double that of the corresponding carbonaceous materials with similar surface area. Further increase of the B content in the $BC_6$ material—having a smaller specific area 609 $m^2/g$—shows 0.54 wt% and 3.8 wt % hydrogen adsorption at 273 and 77K, respectively. Despite the reduction of surface area, the overall hydrogen adsorption capacity clearly increases. Evidently, the substituted B elements are essential in hydrogen adsorption, which enhances the surface energy for binding hydrogen. The quantitative $H_2$ binding energy on the $BC_{11}$ and $BC_6$ materials was estimated by adsorption isotherms (at 77 and 87 K) under low hydrogen pressure (<1 bar). The volume adsorbed at different pressures was converted to heat of adsorption by using Clausius-Clapeyron equation. The initial isosteric heat of adsorption for $BC_{11}$ (run A-1) and $BC_6$ (run C-1) is 12.47 and 20 kJ/mol, respectively. Both samples maintain quite high adsorption energy levels (>10 KJ/mol) to higher surface coverage. They are significantly higher than those observed in undoped

carbonaceous materials (4 kJ/mole) and some metal-doped C materials, and the increase of boron content increases the hydrogen binding energy.

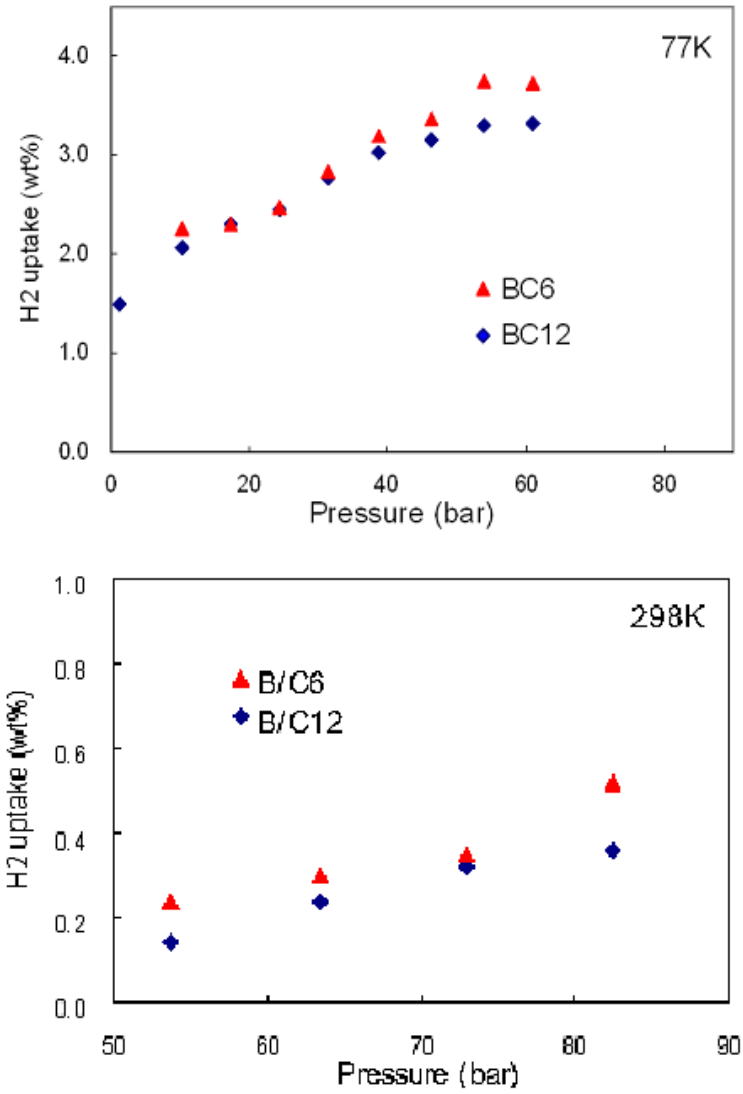


(b) (a)

**Figure 9:** Hydrogen adsorption (vs. $H_2$ pressure) for two porous $BC_6$ (run C-1) and $BC_{12}$ (run A-1) materials at (a) 77K and (b) 293K.

In addition to optimizing geometric structures to improve storage properties, the team also pioneered the use of multiple-element materials to improve dihydrogen binding. In good agreement with theoretical models [2], B substituted with an $sp_2$ structure in carbon enhances hydrogen binding to ~11 kJ/mol [3]. The main issues were (and are) the need to substantially increase the B concentration while maintaining a high specific surface area. In this regard, the HSCoE investigated the use of several synthetic techniques to address issues including pyrolisis of BC precursor materials, templating

$BC^3$, and chemical replacement processes. Similarly, APCI investigated the use of F to enhance dihydrogen binding. The overarching goal of this work was to increase the isosteric heats of adsorption so that temperatures approaching ambient could be used for storage. Increasing the storage temperature reduces system costs and thus provides a potential path to meeting the DOE targets.

We also incorporated substitutional boron in high surface area microporous carbon by pyrolysis of blend of microporous forming polymer precursor (polyfurfuryl alcohol) and boron containing organic precursor (tetraethylammonium borohydride). The as-prepared pyrolyzed sample had 1 – 5 wt% of boron incorporated in them. However, upon activation with $CO_2$, there was selective removal of carbon increasing the amount of boron to almost 23 wt% with surface area of 1500 $m^2/g$. The isosteric heat of adsorption of the sample was ~ 10 KJ/mol with a sorption capacity of 0.5 wt% at room temperature and 100 bars.

Air Products' computational modeling results confirmed that B-substituted carbon would be effective as a hydrogen storage material by direct adsorption of hydrogen or as a hydrogen spillover receptor. Current methods of producing boron-substituted carbons have been moderately successful in increasing material surface area while incorporating high levels of boron substitution. However, a step-change increase in the surface might be realized with the application of templating methods to the existing B-precursor pyrolysis. Therefore, methods were developed to impregnate known precursors into porous silica materials and etch the silica with a minimal amount of boron loss.

The Penn State team also used high surface area mesoporous templates such as silica aerogel, activated carbon and templated carbons as supports to deposit thin films of BCx using chemical vapor deposition technique. Thin films with $sp^2$ boron content as high as 17 atomic% determined using solid state $B^{11}$ NMR and X-ray Photoelectron Spectroscopy was deposited by vapor phase decomposition reaction of boron trichloride and benzene at 900 C. The surface area of the samples after the deposition of BCx was about 250 – 600 $m^2/g$. Isosteric heat of adsorption as high as 12 KJ/mol was observed for BCx coated silica aerogel and high surface area activated carbons. This showed substantial increase as compared to a very low heat of adsorption (~ 4 KJ/mol) for the high surface area supports.The maximum hydrogen uptake for the $BC_x$ coated sample was 1.6 wt% at 77 K and 1 bar.

The Pennsylvania State University team aimed at optimizing the boron contents of both microporous boron-substituted carbons (Mike Chung) and nanoporous carbons with and without boron (Hank Foley and Ramakrishnan Rajagopalan). Prompt-gamma activation analysis was used as a characterization tool to measure the boron content in the synthesized carbons from polymer blends of polyfurfuryl alcohol and tetraethylammonium borohydride. Depending upon the composition of the blends of tetraethylammonium borohydride and polyfurfuryl alcohol, 1 – 5 wt% of boron was detected in the as-prepared samples. The samples were then systematically activated using carbon dioxide at 900 C and the amount of boron content in the sample was measured using PGAA. In general, the boron content in the sample increased dramatically with the extent of activation. Samples with boron content as high as 23 wt % were obtained using this approach.

Additional small-angle neutron scattering (SANS) and inelastic neutron scattering (INS) measurements on nanoporous carbons have been used to gain insights into the morphology of the pore structure and how hydrogen is adsorbed into these materials, in collaboration with NIST (Brown). Due to its light mass, a hydrogen molecule is a good quantum rotor whose transition energy from $J = 0$ to $J = 1$ is about 14.7 meV, where $J$ is the quantum rotation number[1]. When a hydrogen molecule is adsorbed on a material surface, the local interaction potential generated by the host will hinder the rotation resulting in a splitting of the degenerate $J = 1$ energy levels. With low hydrogen loadings on nanoporous carbon (NPC) derived from blends of polyfurfuryl alcohol and polyethylene glycol, there is a clear splitting of the 14.7 meV indicating a relatively strong interaction of adsorbed hydrogen with the carbon material. Until 0.8 wt% hydrogen loading, the split feature is very clear, however, at 1.6 wt% hydrogen loading the spectrum begins to become narrower and centered around 14.7 meV. At the largest loading of 4.2 wt%, the rotational transition peak exhibits one peak with a much smaller full-width at half-maximum (FWHM) of ≈ 1.46 meV. This transition from a split feature in the rotational transition peak to an apparent one peak suggests that the local environment of the adsorbed hydrogen molecules has changed dramatically between 0.8 wt% loading and 1.6 wt% loading. The split feature we observe at low coverage indicates that the rotation of hydrogen molecules adsorbed in the NPC sample is strongly hindered because of the adsorption of hydrogen molecules in the nano-pores less than 1 nm. The INS peak character change between 0.8 wt% and 1.6 wt% indicates that hydrogen molecules continue to be adsorbed in larger pores with lower curvature of the graphitic walls and the rotation of hydrogen molecules are much less hindered.

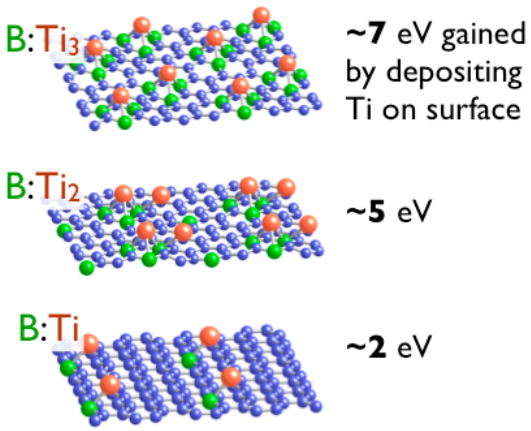


Theory calculations reveal that metal atoms of diverse types can be stabilized in atomically dispersed form through boron-doping of a carbon support, as depicted in the figure above for Ti. Increased boron content increases the stabilization energy with a layer of atomically dispersed metals is added to a boro-carbon sheet.

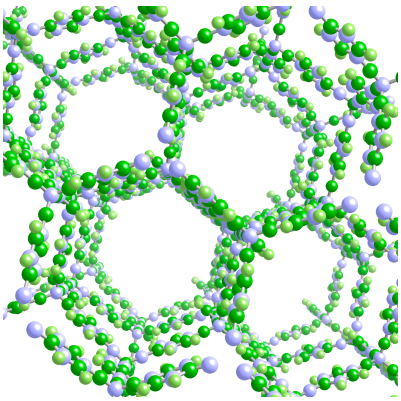

**Figure 10**: A BN-based covalent framework compound, designed to maintain the favorable H-binding energetics of the B-N analogs of hydrocarbons while avoiding the irreversible transformation into ceramic BN. This framework contains borazine-like units inserted into the linkers.

Framework compounds that borrow concepts from covalent organic linker materials but with BN-based linkers were designed which may be capable of storing hydrogen while circumventing two of the primary problems of traditional BN-based hydrogen storage techniques: slow kinetics and irreversible dehydrogenation. The framework structure is designed to suppress the collapse of the structure into ceramic BN, while strains built into the system may be able to reduce the kinetic barriers against hydrogen release and recharge. Molecular dynamics simulations indicate that certain structures in this class are moderately thermally stable and may merit further development.

Theory work has also demonstrated that topologically frustrated charge transfer systems can stabilize dispersed metals. In one test system with Fe dispersed on one side of the carbon sheet and halogen on the other side, enhanced charge transfer due to halogen can enhance the stability of the dispersed state, a requirement for obtaining a large effective surface area for hydrogen adsorption. These systems, designed in computation, provide novel synthetic targets for the future.

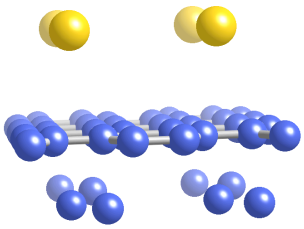

**Figure 11:** Fe dispersed on a graphene sheet with a halogen stabilization unit on the opposing side.

**Papers and Presentations (selected):**

Youmi Jeong and T. C. Mike Chung. "Super-activated Carbon Containing Substitutional Boron ($BC_x$): Synthesis, Characterization, and Applications in Hydrogen Storage" Carbon 2010, 48, 2526-2537.

Youmi Jeong and T. C. Mike Chung. "Mono-Dispersed Transition Metal Nanoparticles on Boron-Substituted Carbon Support"

Hugo E. Romero, Humberto R. Gutierrez, and Peter C. Eklund. "Adsorption of Closed-Shell Aromatic Molecules on Graphene Devices"

Hugo E. Romero, Humberto R. Gutierrez, and Peter C. Eklund. "Interactions Of Aromatic Compounds With Graphene" APS March Meeting 2009

Mono-dispersed transition metal nanoparticles on boron-substituted carbon support and applications in hydrogen storage, Youmi Jeong and T. C. Mike Chung

“Preparation and characterization of high surface area BCx carbon” Carbon 2010 conference, July 11 -16, Clemson, USA and manuscript of the same name.

New energetic regimes for carbon and borocarbon nanostructures: the bi-ribbon, incommensurate stacking in bi-layers and the bi-continuum, Lausanne, Switzerland, 2009.

Electron deficiency stabilizes atomic dispersions of metals on $sp^2$ boro-carbon sheets., Zhoahui Zhang and Vincent Crespi.

Poster Development of nanoporous carbon based shape selective catalyst and potential hydrogen adsorbent materials Energy Innovation Forum, Penn State University, October 23, 2008.

Synthesis of high surface area nanoporous carbon materials with high heats of adsorption of hydrogen, R. Ramagopalan and H. Foley.

The Theory of Chemical Frustration in Hydrogen Storage, V. Crespi et al. Invited talk at MRS Spring Meeting, San Francisco, CA

Poster Development of nanoporous carbon based shape selective catalyst and potential hydrogen adsorbent materials Energy Innovation Forum, Penn State University, October 23, 2008.

A new energetic regime for carbon nanostructures: the bi-ribbon and graphene as a bi-continuum, V. Crespi et al, Invited talk at IMRC Cancun, 2008.

A simple approach to synthesize nanoporous carbons with high heats of adsorption of hydrogen, R. Rajagopalan and H. Foley

Two presentations were given at the January Center meeting in Golden, CO, by Chung and Crespi.